AGU PUBLICATIONS

Geophysical Research Letters

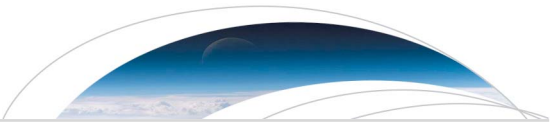

RESEARCH LETTER

10.1002/2015GL066946

Key Points:

- Buoyant plumes in porous media have a complex plume head
- 0.7 of the source material flows into the plume head
- Plume head concentration decreases with flow rate

Correspondence to:
A. W. Woods,
andy@bpi.cam.ac.uk

Citation:
Lyu, X., and A. W. Woods (2016), Experimental insights on the development of buoyant plumes injected into a porous media, *Geophys. Res. Lett.*, *43*, 709–718, doi:10.1002/2015GL066946.

Received 9 NOV 2015
Accepted 16 DEC 2015
Accepted article online 18 DEC 2015
Published online 29 JAN 2016

Experimental insights on the development of buoyant plumes injected into a porous media

Xiaoying Lyu[1,2] and Andrew W. Woods[1]

[1] BP Institute, University of Cambridge, Cambridge, UK, [2] School of Chemical Engineering and Technology, State Key Laboratory of Chemical Engineering, Tianjin University, Collaborative Innovation Center of Chemical Science and Chemical Engineering, Tianjin, China

Abstract We describe a series of new laboratory experiments which examine the rise of a two-dimensional buoyancy-driven plume of freshwater through a porous layer initially saturated with aqueous saline solution. Measurements show that the plume head accounts for a constant fraction of about 0.7 of the buoyancy supplied at the source and that it grows as it rises through the porous layer. However, the morphology of the plume head becomes increasingly complex as the ratio of the injection speed to the buoyancy rise speed increases, with the fluid spreading laterally and developing localized buoyant fingers which intermingle with the ambient fluid. Behind the plume head, a tail of nearly constant width develops providing a pathway from the source to the plume head. These starting plume dynamics may be relevant for buoyancy-driven contaminant dispersal and also for the convection which develops during CO_2 sequestration as CO_2 dissolves into aquifer water.

1. Introduction

A steady source of relatively dense or buoyant fluid in a saturated porous layer can lead to formation of a convective plume which either falls or rises through the ambient fluid. The transient flow associated with such a source of buoyancy is of great interest for several applications including the modeling of the dispersion of a localized source of contaminant in a buoyant flow, water recharge in geothermal systems [*Woods*, 1999; *Menand et al.*, 2003], and, in the context of CO_2 sequestration, modeling the dispersal of a dense plume of CO_2-saturated water produced following dissolution of the CO_2, as it descends through the underlying aquifer [*Riaz et al.*, 2006; *Pau et al.*, 2009; *Unwin et al.*, 2015]. The transient buoyancy-driven flow involves formation of a plume head, which mixes with the ambient fluid, followed by a more localized tail. Prediction of the area swept by the head may be important, for example, if contaminants transported by the flow are adsorbed onto the porous matrix.

There is a significant literature concerning the buoyancy-driven transport of fluid through porous media and, in particular, the dynamics of gravity currents in which dense fluid displaces a less dense fluid as it advances over a horizontal or inclined boundary [*Barenblatt*, 1996; *Huppert and Woods*, 1995; *Woods*, 2015]. Models have also been developed to describe the long-term dispersive mixing of such gravity-driven flows in confined aquifers, based on the ideas of shear dispersion [*Taylor*, 1953; *Perkins and Johnston*, 1963; *Rubin*, 1974, 1975; *Dagan*, 1989; *Schiedegger*, 1974]. This work is of particular relevance in the field of CO_2 sequestration for establishing mixing rates between CO_2 saturated and unsaturated aquifer water [*Szulczewski et al.*, 2013; *Unwin et al.*, 2015]. There is also a vast body of research relating to thermal convection in porous media which results when a horizontal or vertical boundary is heated [*Lapwood*, 1948; *Horton and Rogers*, 1945; *Nield and Bejan*, 2006; *Wooding*, 1957, 1963; *Elder*, 1967; *Hewitt et al.*, 2014]. Depending on the Rayleigh number, convection can lead to very effective mixing of the buoyancy within the flow, and convective flows have been the subject of numerous experimental and numerical modeling studies [*Nield and Bejan*, 2006].

There have also been numerous models developed to describe the dispersion and mixing in porous media, especially associated with pressure-driven flows [*Perkins and Johnston*, 1963; *Rubin*, 1974, 1975; *Bear*, 1972; *Scheidegger*, 1974; *Dagan*, 1989; *Woods*, 2015]. On a pore scale, dispersive mixing occurs owing to the tortuous pathway of individual fluid particles around the solid matrix, and the heterogeneities of the porous layer at progressively larger scales also lead to a hierarchy of dispersive processes. As a result, in some cases, the scale of the dispersivity increases with the scale of the flow [*Phillips*, 1991, 2009].

However, there is less work describing the case in which buoyant fluid supplied at the base of a deep porous layer forms an ascending buoyant plume. *Wooding* [1963, 1957] presented a now classical solution for the dynamics of a buoyancy-driven plume in the case that the cross-flow diffusion of solute or heat is balanced by the downstream advection, leading to a steady self-similar plume structure which grows downstream. This steady regime relies on the lateral diffusion balancing the advection. Since the lateral diffusion is typically very small, the flow may need to travel a considerable distance downstream for this regime to become established. In such cases, in the near-source region, the quasi-steady motion which develops following the passage of the head of the plume may be described using the simplification that there is negligible mixing between the injected and original fluid. For a two-dimensional flow, as may develop from a horizontal line well, this leads to the prediction that the tail of the flow has speed, u_b, and width, w, which depend on the buoyancy $g' = \Delta\rho g/\rho_0$ and the flux of the injected fluid, Q, per unit distance along the well, according to the relations

$$u_b = \frac{kg'\rho_0}{\mu} \quad \text{and} \quad w = \frac{Q}{u_b} \tag{1}$$

where $\Delta\rho$ is the density difference between the ambient saline solution and the injected freshwater. If the source lies within the porous layer, then the flow will adjust to this steady plume regime over a distance of order w above the source. The adjustment process may be described using complex potential theory. *Woods* [2015, section 10.3, equation (10.21)] shows that the boundary between the buoyant source fluid and the surrounding, static ambient fluid has a steady shape described by

$$y = -\frac{Q}{\pi u_b}\left[0.5\ \ln\left(1+\tan^2\left(\frac{\pi u_b x}{Q}\right)\right) - \ln 2\right] \tag{2}$$

with y directed upward and x in the horizontal direction. As the fluid moves downstream from the source, the flow then adjusts to a parallel flow of width w, as above. At long times, once the head has advanced far ahead of the source, this parallel flow will gradually adjust to the self-similar Wooding solution over a distance $u_b w^2/D$ as given by the vertical speed u_b and the time w^2/D for lateral diffusion over a width w.

1.1. The Plume Head

Although the steady flow can be characterized as above, the initial transient flow of the head of the plume is rather different and can involve very substantial intermingling and mixing of ambient fluid with the buoyant fluid in the head of the flow. In turn, this leads to a much wider, laterally spreading and ascending region of reduced buoyancy. There has been less work reporting on the structure of such a plume, and the purpose of this paper is to present a series of new small-scale laboratory experiments which characterize the mixing into the head of such a flow and to establish some insight into the controls on the mixing. We describe the experimental method and present some observations of the structure of the flow as several key properties of the flow are changed. This leads to a new picture of the complexity of the mixing and dispersion in the plume head.

2. Experimental Method

A series of experiments to examine the ascent of a buoyant plume through a two-dimensional porous bed were carried out in a tank of dimension 50.0 × 50.0 × 1.1 cm. The tank was filled with glass ballotini, either of size 3 mm or of size 1.4 mm. The porous layer was then filled with a saline solution with concentration which was varied between experiments, with values in the range 38–166 ppt. Finally, freshwater was supplied to an inflow port in the base of the tank at a constant rate, in the range 0.19–6.13 cm^3/s. The tank was backlit with a light sheet of dimensions 82.0 × 51.0 cm. The light sheet was composed of a 10 mm thick Opal 030 Acrylic Light Diffuser with 12v(5300k) LEDs embedded in the two long sides. Images of the light intensity at the front of the tank were then measured using a Canon D90 camera using the settings : ISO 200, F 5.6, and shutter speed 1/50s.

Prior to the main experiments, the light intensity associated with mixtures of freshwater and fluid-containing different masses of dye were measured at each point on the front face of the tank. By averaging over squares, each of area 3 × 3 mm, corresponding to 23 × 23 pixels, a calibration curve was generated to relate the light intensity to the mass concentration of dye. In the main experiments, dye of a known mass was added to the injected water. As the water spread through the bead pack, displacing and mixing with the original fluid, the calibration curve could then be used to determine the local buoyancy of the fluid, $g' = g\beta\Delta s$ where

$\Delta s = s_a - s_p$, the difference between the salinity in the ambient and the plume. In each experiment, we compared the total buoyancy of the water supplied to the tank with an estimate of the total buoyancy of the fluid in the tank as obtained from the imaging. We found that the two values agreed within a factor of 10% through the experiment. Some of this error is associated with the challenge of thresholding the boundary of the plume where there may be thin dispersed layers of the buoyant fluid and this led to a systematic underprediction of the mass of dye in the tank; error bars consistent with this underestimate are included in our experimental measurements. In our analysis, we use estimates for the porosity and permeability of the porous layer. The porosity was measured directly by measuring the volume of water required to fill the pore space, while the permeability was found by measuring the speed of a gravity-driven draining flow. This measured permeability was in very good accord with the prediction from the Kozeny-Carmen equation.

3. Experimental Results

Images of the morphology and buoyancy of the plume were analyzed to determine the key features of the flow and to explore how these changed as the experimental parameters were changed. The list of experiments conducted are included in Table 1. In order to classify the behavior in the experiments, it is useful to consider the dimensionless parameters which may control the flow. In this context, there are two characteristic speeds in the problem, corresponding to the injection speed, u_0, defined as the source volume flux divided by the product of the cross-sectional area of the inflow port and the buoyancy rise speed, u_b, based on the initial salt concentration (equation (1)). We have therefore explored the dependence of the flow on their ratio, $F = u_0/u_b$; in our experiments F spanned the range $1 < F < 20$.

First, in Figure 1 we present a time series of photographs of the development of a typical plume, showing (a) actual photographs of the dyed plume and (b) false color images which illustrate the variation of the buoyancy of the plume, as determined from the light attenuation measurements. It is seen that the plume head develops a very complex structure, breaking up into a series of individual lobes, which advance upward at different rates. Each of the lobes appears to carry relatively buoyant fluid similar to that of the supply fluid. In each case, behind the head, a simple, nearly parallel sided tail develops, with a sharp near vertical transition from the buoyant source fluid to the ambient fluid.

In order to gain more insight into the mixing and flow morphology, in Figure 2 we present a time series of a second experiment in which we changed the color of the dye in the input fluid several times during the experiment. In order to change the dye color, we had two reservoirs of source fluid, one containing blue and one containing red dye. We used a three-way valve on the inflow supply pipe to the pump which is connected to the experimental tank. We were then able to switch the supply fluid between the two sources. As the plume develops, it is seen that fluid in the tail advances more rapidly than the plume head and so the head is continually supplied with new buoyant fluid. This new fluid rises through the head to the leading edge of the plume, where it enters one or more of the lobes, becomes diluted and is eventually overtaken by further parcels of fluid supplied from the tail. As a result of the greater flow speed in the tail of the plume compared to the head, the total area and the total buoyancy of the head increase with time. Indeed, Figure 2a illustrates the advance of the leading and trailing edges of the plume head and of the dyed fluid within the tail. The individual data points correspond to measurements taken from successive photographs of the experiment.

The development of a growing and dispersing plume head may be very significant in the context of contamination of the subsurface, since the plume head appears to pass through a much larger volume of the porous layer than the relatively narrow plume tail, which involves relatively little mixing. We have therefore explored how the overall morphology of the plume head depends on various controlling parameters and find that one key parameter is F. Figure 3 illustrates the shape of the plume head for several values of F; in each case, the image corresponds to the time when the front of the head had reached a distance 40 cm ahead of the source. With a small value of F corresponding to a relatively small initial flow speed compared to the buoyancy speed, the plume head rises as a relatively localized plume structure. In this case, the plume head slowly spreads laterally as it rises and the buoyancy decreases as it mixes with the ambient fluid. This flow gradually adjusts toward the Wooding type flow (Figure 3). However, for larger values of F, corresponding to progressively larger values of the initial flow speed relative to the buoyant rise speed, the plume width w increases, and the flow tends to spread laterally as it rises through the formation. As the flow displaces the ambient fluid it decelerates, widens, and appears to become unstable breaking up into a series of fingers of increasingly

Table 1. Table of Experiments[a]

Experiment	Salinity (ppt)	ρ_a (kg/m^3)	Q (cm^2/s)	ϕ	k ($\times 10^{-9}$ m^2)	u_b (cm/s)	F
1.1	20	1012.97	0.11	0.41	9.6	0.14	2.76
1.2	20	1012.97	0.19	0.41	9.6	0.14	4.60
1.3	20	1012.97	0.19	0.41	9.6	0.14	4.63
1.4	20	1012.97	0.3	0.41	9.6	0.14	7.37
1.5	20	1012.97	0.38	0.41	9.6	0.14	9.19
1.6	20	1012.97	0.38	0.41	9.6	0.14	9.26
2.1	38	1027.14	0.18	0.40	8.9	0.25	2.43
2.2	38	1027.14	0.18	0.40	8.9	0.25	2.43
2.3	38	1027.14	0.36	0.40	8.9	0.25	4.85
2.4	38	1027.14	0.36	0.40	8.9	0.25	4.85
2.5	38	1027.14	0.38	0.40	8.9	0.25	5.10
2.6	38	1027.14	0.72	0.40	8.9	0.25	9.59
2.7	38	1027.14	0.73	0.40	8.9	0.25	9.71
2.8	38	1027.14	1.03	0.40	8.9	0.25	13.7
2.9	38	1027.14	1.07	0.40	8.9	0.25	14.3
3.1	57	1040.93	0.38	0.41	9.6	0.40	3.17
3.2	57	1040.93	0.38	0.41	9.6	0.40	3.18
3.3	57	1040.93	0.76	0.41	9.6	0.40	6.27
3.4	57	1040.93	0.76	0.41	9.6	0.40	6.28
3.5	57	1040.93	1.14	0.41	9.6	0.40	9.43
3.6	57	1040.93	1.15	0.41	9.6	0.40	9.50
3.7	57	1040.93	1.46	0.41	9.6	0.40	12.1
3.8	57	1040.93	1.47	0.41	9.6	0.40	12.2
3.9	57	1040.93	1.88	0.41	9.6	0.40	15.6
3.10	57	1040.93	2.29	0.41	9.6	0.40	19.0
4.1	74	1054.34	0.29	0.40	8.9	0.49	1.98
4.2	74	1054.34	0.31	0.40	8.9	0.49	2.11
4.3	74	1054.34	0.37	0.40	8.9	0.49	2.54
4.4	74	1054.34	0.38	0.40	8.9	0.49	2.60
4.5	74	1054.34	0.61	0.40	8.9	0.49	4.15
4.6	74	1054.34	0.61	0.40	8.9	0.49	4.15
4.7	74	1054.34	0.76	0.40	8.9	0.49	5.21
4.8	74	1054.34	0.77	0.40	8.9	0.49	5.27
4.9	74	1054.34	0.91	0.40	8.9	0.49	6.20
4.10	74	1054.34	0.92	0.40	8.9	0.49	6.26
4.11	74	1054.34	1.54	0.40	8.9	0.49	10.5
4.12	74	1054.34	1.54	0.40	8.9	0.49	10.5
4.13	74	1054.34	2.3	0.40	8.9	0.49	15.7
4.14	74	1054.34	2.3	0.40	8.9	0.49	15.7
5.1	91	1070.52	0.37	0.40	8.9	0.63	1.98
5.2	91	1070.52	0.37	0.40	8.9	0.63	1.98
5.3	91	1070.52	0.74	0.40	8.9	0.63	3.92
5.4	91	1070.52	0.75	0.40	8.9	0.63	3.97
5.5	91	1070.52	0.76	0.40	8.9	0.63	4.01
5.6	91	1070.52	1.09	0.40	8.9	0.63	5.80
5.7	91	1070.52	1.13	0.40	8.9	0.63	6.00
6.1	167	1130.24	0.17	0.40	8.9	1.08	0.52
6.2	167	1130.24	0.37	0.40	8.9	1.08	1.14
6.3	167	1130.24	0.39	0.40	8.9	1.08	1.19
6.4	167	1130.24	0.82	0.40	8.9	1.08	2.55
6.5	167	1130.24	1.23	0.40	8.9	1.08	3.82
6.6	167	1130.24	1.57	0.40	8.9	1.08	4.87
6.7	167	1130.24	1.63	0.40	8.9	1.08	5.06
6.8	167	1130.24	2.09	0.40	8.9	1.08	6.49
6.9	167	1130.24	2.36	0.40	8.9	1.08	7.30
6.10	167	1130.24	5.53	0.40	8.9	1.08	17.1
6.11	167	1130.24	5.57	0.40	8.9	1.08	17.3

Table 1. (continued)

Experiment	Salinity (ppt)	ρ_a (kg/m^3)	Q (cm^2/s)	ϕ	k ($\times 10^{-9}$ m^2)	u_b (cm/s)	F
7.1	74	1054.34	0.11	0.36	1.2	0.068	5.63
7.2	74	1054.34	0.15	0.36	1.2	0.068	7.36
7.3	74	1054.34	0.19	0.36	1.2	0.068	9.20
7.4	74	1054.34	0.30	0.36	1.2	0.068	14.7
7.5	74	1054.34	0.37	0.36	1.2	0.068	18.3
7.6	74	1054.34	0.50	0.36	1.2	0.068	24.5
7.7	74	1054.34	0.57	0.36	1.2	0.068	27.9

[a]In experiments 1 – 6, bead size is 3 mm, in experiments 7, bead size is 1.4 mm.

complex morphology. During the evolution of the flow, the buoyancy in the fingers appears to remain relatively high, so that although there is a complex intermingling of the fluids, there is in fact less mixing with the ambient fluid. Following behind the head of the current, the tail develops as a relatively simple structure of nearly constant width and buoyancy equal to that of the unmixed source fluid. This source fluid rises through the growing tail until eventually supplying new buoyant fluid to the head (Figure 2). This trend in the morphology and mixing in the plume head as F increases occurs both in experiments with beads of size 3 mm (Figure 3a) and also 1.5 mm (Figure 3b).

In order to gain some quantitative understanding of the flow, we have calculated the area and buoyancy of that part of the plume head which contains buoyant fluid, corresponding to the lobes or fingers in the head. Using this data, we can then calculate the average buoyancy, and hence, the degree of mixing of the buoyant fluid in the plume head as a function of time for the series of experiments shown in Table 1. We first find the integral of the buoyancy across a horizontal line through the plume

$$\overline{g}(z) = \int_{-L}^{L} g'(x,z)\mathrm{d}x \tag{3}$$

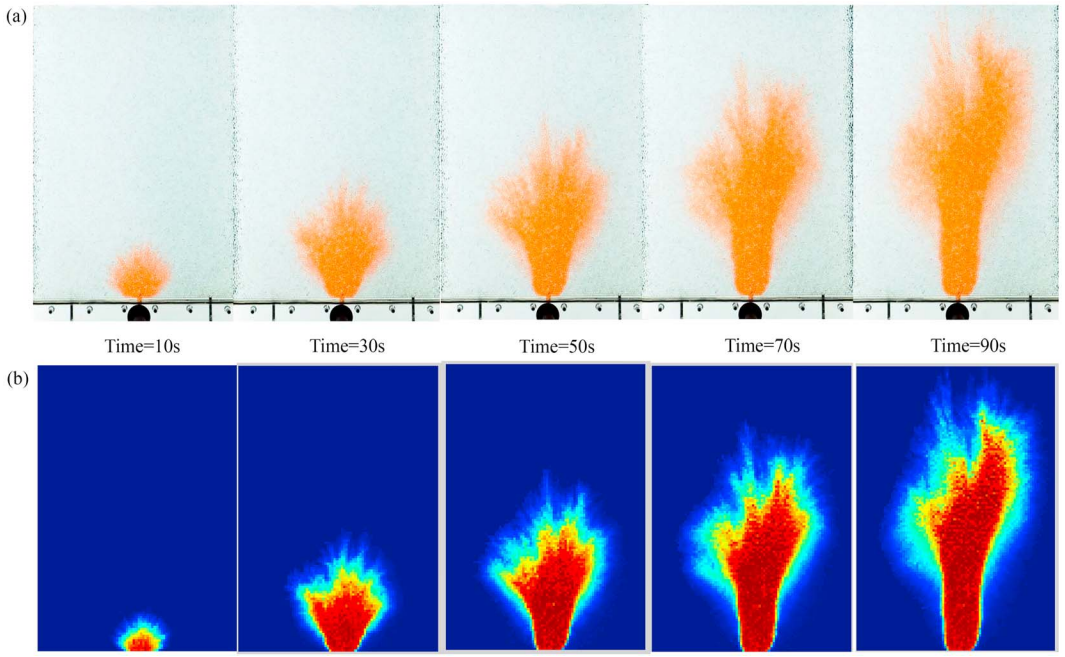

Figure 1. (a) Photographs of buoyant plume of freshwater rising from a point source into a tank of saline water. In Figure 1a photographs show the original dyed plume rising into the ambient while (b) photographs show the false color images corresponding to the salinity of the plume. Photographs correspond to Experiment 1.1 in Table 1.

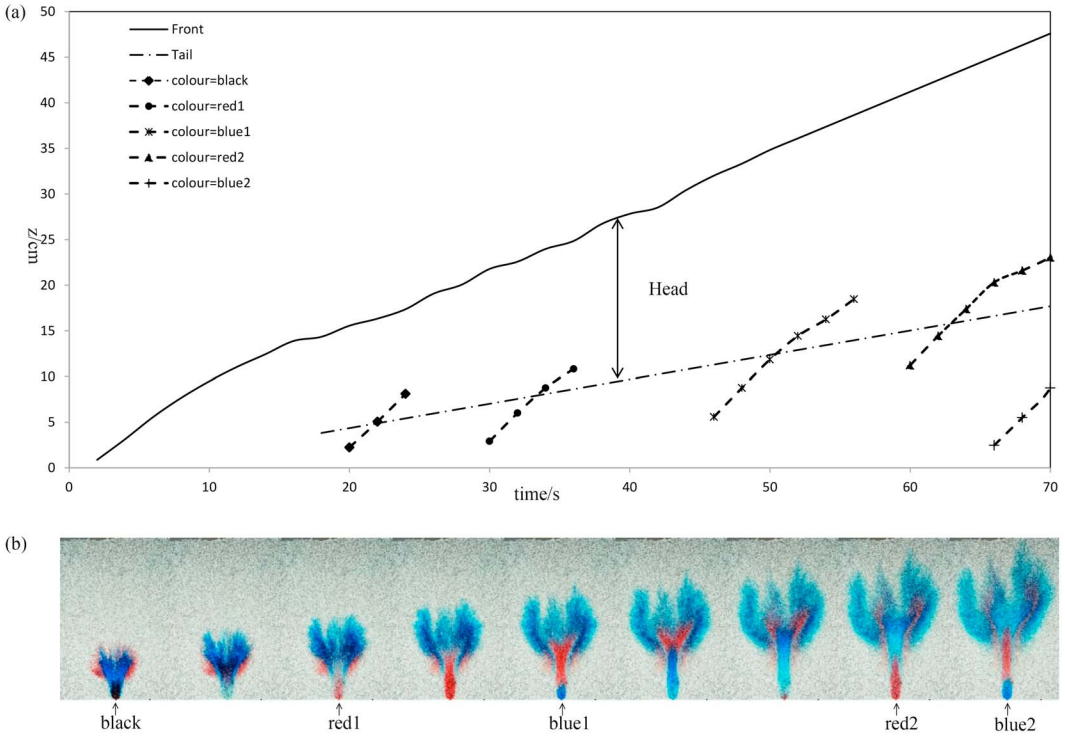

Figure 2. Series of images of a plume in which the color of the dye was successively changed in order to help visualize the migration of the fluid from the tail into the head. Here the fluid reaches the front of the flow, mixes, and is then overtaken by further dyed fluid from the tail. In this experiment, we used 3 mm beads, 91 ppt salinity water, and $Q = 0.80\,cm^2/s$.

We then take the vertical average of $\overline{g}$ by integrating along a vertical line which originates at the source and extends up to height z

$$\hat{g}(z) = \frac{1}{z}\int_0^z \overline{g}(z)dz \tag{4}$$

As we move from the tail into the head, we expect that $\overline{g}(z)$ increases to values substantially larger than $\hat{g}(z)$. At each time t we can then define the transition point from the head to the tail as that point $z = z_c(t)$ at which

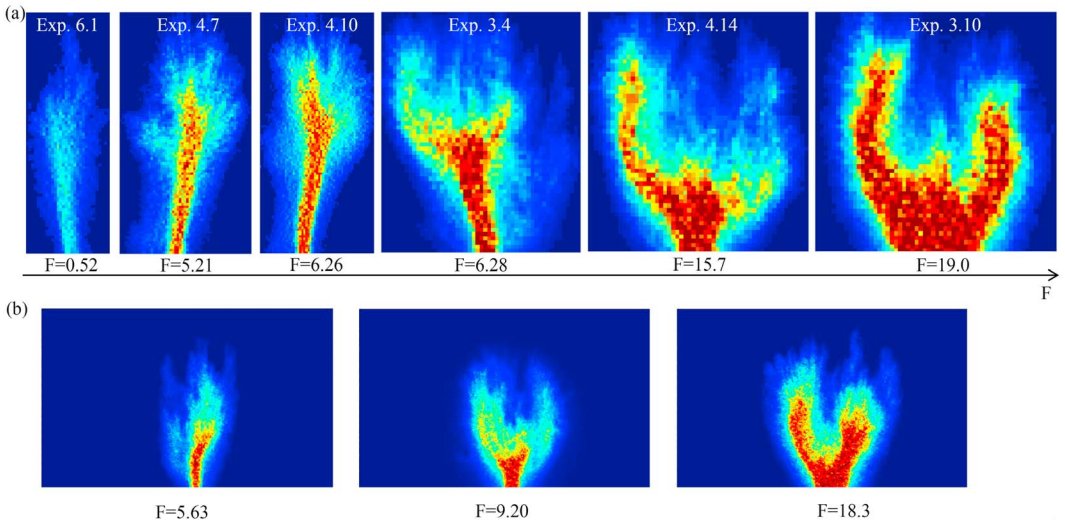

Figure 3. Morphology of the plume head, arranged in an order of increasing F. (a) A series of experiments using beads of size 3 mm while (b) from beads of size 1.4 mm.

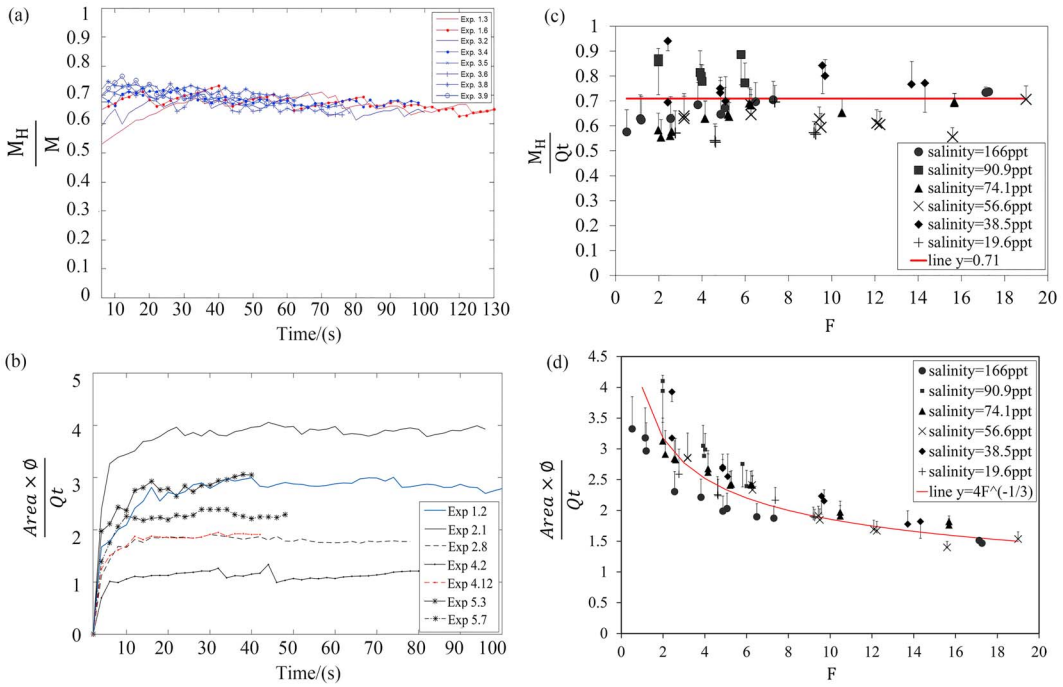

Figure 4. (a and c) Variation of the total buoyancy in the plume head as a fraction of the total buoyancy injected into the tank. Figure 4a shows variation with time, for several experiments as indicated in legend, and Figure 4c shows variation of the time average as a function of F. The solid red line has value 0.71. (b and d) Variation of the total area of buoyant fluid in the plume head divided by the total volume of fluid injected into the cell per unit thickness of the cell. Figure 4b shows variation with time, for several experiments as indicated in the legend, and Figure 4d shows variation of the time average as a function of F. The solid red line shows the curve $4F^{-1/3}$.

$R(z_c) = R_c$ where we define

$$R(z,t) = \overline{g}(z,t)/\hat{g}(z,t) \tag{5}$$

The critical value R_c delineating the transition from the tail to the head is somewhat arbitrary, but we find that the value $R_c = 1.3$ provides a robust estimate of the location of the transition since in the tail, $R(z)$ has values in the range 0.8–1.2, while in the head R_c increases to values much in excess of 1.4. We define the top of the plume head as that point $z = z_t > z_c$ at which $R(z_t) = 0.05$. Analysis of the data shows that these thresholds provide a robust parametrization distinguishing the tail and head of the plume.

In Figure 4, we illustrate the variation with time of (a) the buoyancy in the head as a fraction of the buoyancy supplied from the source and (b) the volume of fluid in the head which contains relatively saline fluid, as a fraction of the volume of fluid supplied to the cell. The volume is estimated by adding the area of those pixels in the head for which the concentration is in excess of the background value, in the region $z_c < z < z_t$, and multiplying by the depth of the cell times the porosity. Figures 4a and 4b show the variation with time in a series of experiments, while Figures 4c and 4d show the time average as a function of F. The data suggest that a nearly constant fraction 0.7 ± 0.1 of the buoyancy supplied to the system enters the head of the flow, for all the experiments with $1 < F < 20$. The buoyancy data are consistent with the base of the plume head rising at a speed of order 0.3 ± 0.1 of the interstitial speed of the fluid in the tail of the plume, as given by the buoyancy rise speed, u_b/ϕ (see below).

The data (Figure 4b) also suggest that after a very short initial transient, the volume of buoyant fluid in the head of the two-dimensional plume increases at a nearly constant rate, with the ratio of this volume as a fraction of the input volume flux ranging from about 4 to 1 depending on F. Figure 4d suggests that the time-averaged volume as a fraction of the input volume flux varies with F as $F^{-1/3}$. This figure illustrates that the tendency for the plume head to spread laterally and develop a number of discrete, high-buoyancy fingers for large values of F (Figure 3) leads to less mixing of the input fluid with the ambient fluid than in the case of smaller F for which the plume head remains more localized but for which the fluid appears to mix more with the ambient fluid (Figure 3). Indeed, using the above data, we have calculated the mean buoyancy in that part of the plume

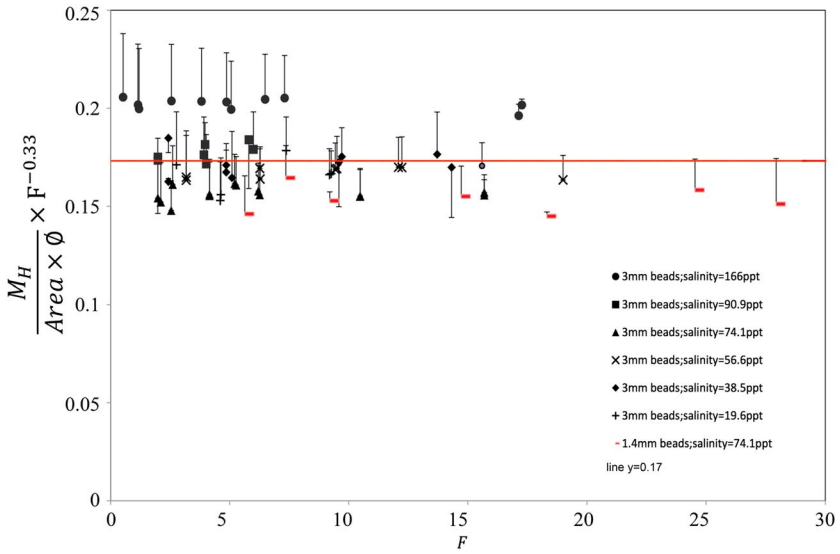

Figure 5. Variation of the product of $F^{-1/3}$ and the spatially averaged buoyancy of the buoyant fluid in the plume head, as a fraction of the buoyancy of the fluid injected into the cell, shown as a function of F.

head which contains buoyant fluid. This is defined as

$$g' = \frac{\int_{z_c}^{z_t}\int_{L_-}^{L_+} g' \mathrm{d}x\mathrm{d}z}{\int_{z_c}^{z_t}\int_{L_-}^{L_+} \mathrm{H}(g'>0)\mathrm{d}x\mathrm{d}z} \tag{6}$$

where L_- and L_+ are the horizontal locations of the plume furthest from the center of the plume to the left and right, respectively. For each experiment, we then found the time average of g', defined to be g', and in Figure 5 we show that this follows a consistent trend with F, given by the scaling

$$\overline{\hat{g}'} = g'_o(0.17 \pm 0.02)F^{(1/3)} \tag{7}$$

for $1 < F < 20$, where g_o is the buoyancy of the fluid supplied to the system. In the figure, we have included some error bars, which are based on a comparison of the known mass of dye injected into the tank and the mass of dye in the tank as estimated using the light attenuation technique; in some cases, the estimated mass of dye was smaller than the actual mass injected, and so the error bars are shown as being dominantly one sided. As the source buoyancy increases or the source flux decreases, there is an increase in the mixing of the fluid in the plume head with the ambient fluid leading to a lower buoyancy of the fluid in the head.

Although the dynamics of the plume head are complex, with the degree of mixing in the plume head depending critically on the morphology of the head, the tail has a much simpler structure. In each experiment, analysis of the tail suggests that it remains nearly parallel sided, and there is only a narrow boundary layer region on the edge of the plume across which the buoyancy adjusts from the input buoyancy to the ambient. The fluid in the tail of the plume appears to rise with speed u_b, with relatively little mixing until after it has entered the more dispersed head of the plume.

4. Discussion

The experiments described in this work identify that when a localized source of buoyant fluid is supplied to a porous medium saturated with a fluid in which the buoyant fluid is miscible, the flow develops a plume head and tail structure, with an expansive head region, which spreads laterally as well as upward, while the tail of the flow remains of nearly constant width and is controlled by the volume flux and buoyancy-driven rise speed of the source fluid. The plume head receives a fraction of about 0.7 ± 0.1 of the buoyancy flux supplied at the source, and this leads to a gradual growth of the head. As the plume head advances, the leading edge of the head develops a series of lobes or fingers which lead to intermingling of the plume fluid and the original fluid in the porous layer. This results in a very complex morphology of the plume head, and a substantial increase in

the area of the porous layer through which the plume head passes. However, although the morphology of the plume head becomes more complex as u_0 increases, the amount of dilution of the fluid within the buoyant fingers decreases with u_0, the speed of the supply fluid at the source. Measurements show that the average buoyancy of the fluid in the plume head in fact follows a law of the form $(0.17 \pm 0.02)g'_o F^{1/3}$ where the ratio F is given by the characteristic speed of the flow at the source, u_0, to the buoyancy speed u_b. These observations apply across a series of experiments for which F lies in the range $1 < F < 20$.

From a dynamical perspective, the speed of the plume head is expected to be smaller than the tail, as it has to displace the ambient fluid ahead of the plume, as the plume advances. Models of the rise of a cylindrical parcel of buoyant fluid in a porous layer predict that the Darcy velocity of the parcel is about one half the buoyancy rise speed $u_b/2$ [cf. *Yih*, 1966]. In the present problem the morphology of the plume head, with the discrete and irregular buoyant fingers leads to a more complex flow pattern around the head. Moreover, the volume of the head slowly grows with time with the plume head accounting for about 0.7 ± 0.1 of the buoyancy supplied to the system. This is consistent with the rear of the plume head ascending with an interstitial speed of order $(0.3 \pm 0.1)u_b/\phi$. Our results imply that on the scale of our experiments, as the plume grows, the speed of the head depends only on the buoyancy speed and is independent of the size of the head. Since this speed is a constant, there is a constant flux of material from the tail entering the head, and hence, the plume head accounts for a fixed fraction of the total buoyancy. The observation that a starting plume rises more slowly than the subsequent steady plume has also been observed in turbulent buoyant plumes, although the dynamics of such plumes are very different from the present situation [*Turner*, 1966].

Although the plume head has a complex morphology which depends on F, the tail of the plume appears to be a somewhat simpler parallel-sided structure, and over the scale of our experiments, the fluid within the tail has concentration equal to the source concentration and it has interstitial velocity u_b/ϕ. We expect that the tail will adjust toward the classical Wooding solution at a distance $L_w = u_b\tau$ ahead of the source, where τ is the time for cross-flow diffusion through the width of the plume, $\tau = w^2/D = Q^2/u_b^2 D$, giving the result $L_w \sim Q^2/Du_b$.

Our results provide insight into the buoyancy-driven motion of a plume of fluid through a porous layer. The local pore scale dispersive mixing and the large-scale formation of fingers from the injected fluid lead to production of a dilute, spatially extensive plume head. If the injected fluid has a contaminant which may adsorb onto the porous layer, this motion of the plume head may lead to formation of a much larger zone of contaminant than the ensuing tail of the plume. The experimental model we have presented has implications for modeling the fate of CO_2 following injection into an inclined saline aquifer as part of a geosequestration scheme. As CO_2 dissolves into the groundwater, perhaps at a structural high where the buoyant CO_2 may accumulate, the resulting CO_2-saturated water will be relatively dense compared to the original groundwater and this may lead to a convective plume spreading downslope through the aquifer. The dispersal and mixing in the plume head, as described herein, may have an important control on the migration and evolution of this CO_2-rich plume and hence on estimates of the long-term dispersion of the CO_2. The experimental results presented herein may also be of interest as a reference for testing numerical models of buoyancy-driven contaminant transport in a porous layer.

Acknowledgments
This work was partially supported by a grant from the Chinese Ministry of Education. Xiaoying Lyu acknowledges support from Jingkang Wang and experimental assistance from Lotty Gladstone.

References

Barenblatt, G. I. (1996), *Scaling, Self-Similarity, and Intermediate Asymptotics*, Cambridge Univ. Press, Cambridge, U. K., doi:10.1017/CBO9781107050242
Bear, J. (1972), *Dynamics of Fluids in Porous Media*, American Elsevier, New York.
Dagan, G. (1989), *Flow and Transport in Porous Formations*, Springer, Berlin.
Elder, J. W. (1967), Transient convection in a porous medium, *J. Fluid Mech.*, *27*, 609–623, doi:10.1017/S0022112067000576.
Hewitt, D. R., J. A. Neufeld, and J. R. Lister (2014), High Rayleigh number convection in a three-dimensional porous medium, *J. Fluid Mech.*, *748*(6), 879–895, doi:10.1017/jfm.2014.216.
Horton, C. W., and F. T. Rogers (1945), Convection currents in a porous medium, *J. Appl. Phys.*, *16*, 367–370, doi:10.1063/1.1707601.
Huppert, H. E., and A. W. Woods (1995), Gravity-driven flows in porous layers, *J. Fluid Mech.*, *292*, 55–69, doi:10.1017/S0022112095001431.
Lapwood, E. R. (1948), Convection of a fluid in a porous medium, *Math. Proc. Cambridge Philos. Soc.*, *44*, 508–521, doi:10.1017/S030500410002452X.
Menand, T., A. Raw, and A. W. Woods (2003), Thermal inertia and reversing buoyancy in flow in porous media, *Geophys. Res. Lett.*, *30*(6), 1291, doi:10.1029/2002GL016294.
Nield, D. A., and A. Bejan (2006), *Convection in Porous Media*, Springer, New York.
Pau, G. S. H., J. B. Bell, K. Pruess, A. Almgren, M. Lijewsji, and K. Zhang (2009), Numerical studies of density-driven flow in CO_2 storage in saline aquifers, paper presented at TOUGH Symposium 2009, Lawrence Berkeley Natl. Lab., Berkeley, Calif. 14–16 Sept.
Perkins, T. K., and O. E. Johnston (1963), A review of diffusion and dispersion in porous media, *J. Soc. Pet. Eng.*, *3*(1), 70–84, doi:10.2118/480-PA.

Phillips, O. M. (1991), *Flow and Reaction in Permeable Rocks*, Cambridge Univ. Press, Cambridge, U. K.
Phillips, O. M. (2009), *Geological Fluid Mechanics: Subsurface Flow and Reactions*, Cambridge Univ. Press, Cambridge, U. K.
Riaz, A., M. Hesse, H. A. Tchelepi, and F. M. Orr (2006), Onset of convection in a gravitationally unstable diffusive boundary layer in porous media, *J. Fluid Mech.*, *548*, 87–111, doi:10.1017/S0022112005007494.
Rubin, H. (1974), Heat dispersion effect on thermal convection in a porous medium layer, *J. Hydrol.*, *21*(2), 173–185, doi:10.1016/0022-1694(74)90035-3.
Rubin, H. (1975), On the analysis of cellular convection in porous media, *Int. J. Heat Mass Transfer*, *18*(12), 1483–1486, doi:10.1016/0017-9310(75)90264-1.
Scheidegger, A. E. (1974), *The Physics of Flow Through Porous Media*, Univ. of Toronto Press, Toronto.
Szulczewski, M. L., M. A. Hesse, and R. Juanes (2013), Carbon dioxide dissolution in structural and stratigraphic traps, *J. Fluid Mech.*, *736*, 287–315, doi:10.1017/jfm.2013.511.
Taylor, G. I. (1953), Dispersion of soluble matter in solvent flowing slowly through a tube, *Proc. R. Soc. A*, *219*, 186–203, doi:10.1098/rspa.1953.0139.
Turner, J. S. (1966), Jets and plumes with negative or reversing buoyancy, *J. Fluid Mech.*, *26*, 779–792, doi:10.1017/S0022112066001526.
Unwin, H. J., G. N. Wells, and A. W. Woods (2015), CO_2 dissolution in a background hydrological flow, *J. Fluid Mech.*, in press.
Wooding, R. A. (1957), Steady state free thermal convection of liquid in a saturated permeable medium, *J. Fluid Mech.*, *2*, 273–285, doi:10.1017/S0022112057000129.
Wooding, R. A. (1963), Convection in a saturated porous medium at large Rayleigh number or Peclet number, *J. Fluid Mech.*,*15*, 527–541, doi:10.1017/S0022112057000129.
Woods, A. W. (2015), *Flow in Porous Rocks: Energy and Environmental Applications*, pp. 1–285, Cambridge Univ. Press, Cambridge, U. K.
Yih, C. S. (1966), *Stratified Flows*, pp. 1–418, Academic Press, New York.